World Academy of Science, Engineering and Technology
International Journal of Mechanical and Mechatronics Engineering
Vol:2, No:5, 2008

Geometry Calibration Factors of Modified Arcan Fracture Test for Welded Joint

S. R. Hosseini, N. Choupani, and A. R. M. Gharabaghi

***Abstract*—**In this study the mixed mode fracture mechanics parameters were investigated for high tensile steel butt welded joint based on modified Arcan test and finite element analysis was used to evaluate the effect of crack length on fracture criterion. The non-dimensional stress intensity factors, strain energy release rates and J-integral energy on crack tip were obtained for various in-plane loading combinations on Arcan specimen starting from pure mode-I to pure mode-II loading conditions. The specimen and apparatus were modeled by finite element method and analyzed under various loading angles (between 0 to 90 degrees with 15 degree interval) to simulate the pure mode-I, II and mixed mode fracture. Since the analytical results are independent from elasticity modules for isotropic materials, therefore the results in elastic fields can be used for Arcan specimens. The main objective of this study was to evaluate the geometric calibration factors for modified Arcan test specimen in order to obtain fracture toughness under mixed mode loading conditions.

***Keywords*—**Arcan specimen, Geometric calibration factors, Mixed Mode, Fracture mechanics.

I. Introduction

IN this study, crack size effects were investigated on steel butt weld fracture properties and geometric calibration factors were calculated for mixed-mode Arcan test specimens. The Arcan apparatus can be tested for in-plane mixed-mode conditions. The geometric parameter are calculated on various crack length ratio and various loading angles. The mixed-mode fracture mechanics aim is to predict critical state under conditions that crack tip deflection are induced under opening (mode-I), in-plane shear (mode-II) and out-plane shear (mode-III) loading, as shown in Fig. 1 [1]. For mixed mode conditions, previous work for mode-I and mode-III fields under small-scale yielding conditions has shown complex behavior, with the in-plane stresses having a different asymptotic functional form than the out-of-plane stresses [2]. Pure mode-I, II and mixed-mode-I/II are more possible in engineering problems. Many tests have been used to measure the fracture toughness. The double cantilever beam (DCB) test [3] and compact tension specimen (CT) [4] are most often used to measure mode-I (opening) fracture toughness for metallic materials.

S. R. Hosseini is with the Civil Engineering Department, Sahand University of Technology, Tabriz, Iran (e-mail: r_hosseini@sut.ac.ir).

N. Choupani is now with the Department of Mechanics Engineering, Sahand University of Technology, Tabriz, Iran (corresponding author to provide phone: +98-412-3459051; fax: +98-412-3444300; e-mail: choupani@sut.ac.ir).

A. R. M. Gharabaghi is with the Civil Engineering Department, Sahand University of Technology, Tabriz, Iran (e-mail: mgharabaghi@sut.ac.ir).

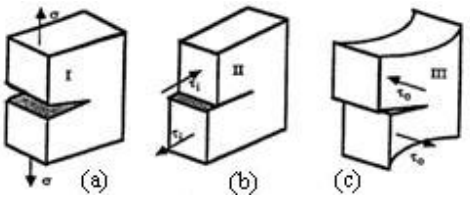

Fig. 1 (a–c) Three basic modes of fracture

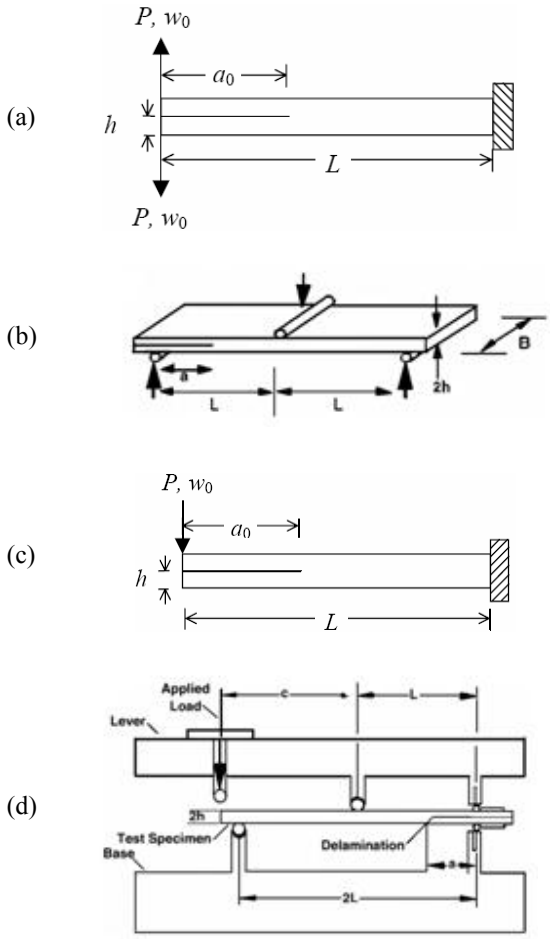

Fig. 2 Most applicable tests, (a) double cantilever beam (DCB) for mode I, (b) end-notch flexure (ENF) and (c) end load split (ELS) for mode II, (d) mixed mode bending (MMB) for mixed mode I&II

The end-notched flexure (ENF) test [5] is most often used to measure mode-II (sliding shear) fracture toughness. However, crack growth in structures is usually not a result of pure mode-I or pure mode-II loading, so it is important that the fracture toughness be known for mixed-mode loading.

Several tests have been used for measuring mixed-mode fracture toughness in the mode-I/mode-II range. These tests include: the edge-delamination tension [6] the crack-lap shear [7], the mixed-mode bending (MMB) test [8], the asymmetric double cantilever beam [9], the mixed-mode flexure [10], and the variable mixed-mode [11] test, some of these tests are shown in Fig. 2. However, all of these tests have one or more problems which limit their usefulness. The modified Arcan test [12] seems to solve many of these problems. The MMB test uses a lever to simultaneously apply mode-I and mode-II type loadings, and by rotating the lever, practically any mode-I/mode-II ratio can be obtained. The Arcan test can be used with the simple and similar specimens for all in-plane mixed-mode tests and can be used to separate the mode-I and mode-II components. In other mixed-mode fracture tests, several different types of specimens are often needed to measured fracture toughness over a desired range of mixed-mode combinations. The use of different test configurations can involve different test variables and analysis procedures that can influence test results in ways that are difficult to predict. The Modified Arcan test can be used to measure fracture toughness over a wide range of mixed mode I/II ratios including pure mode I and pure mode II.

In this research calibration factors of Arcan specimens were calculated via the Arcan apparatus modeling using finite element method and fracture toughness of high tensile steel butt weld was calculated and also the influence of crack length ratio on stress intensity factors and energy released rates for different loading angles were investigated.

II. Finite Element Background

The stress intensity factors, l and *K* plays an important role in linear elastic fracture mechanics. They characterize the influence of the load or deformation on the magnitude of crack tip stress and strain fields and measure the propensity of crack propagation or the crack driving forces. Furthermore, the stress intensity can be related to the energy release rate (the J-integral) for a linear elastic material through

$$J = \frac{1}{8\pi} K^T . B^{-1} \tag{1}$$

where $K = \left[K_I, K_{II}, K_{III}\right]^T$ and B is called the pre-logarithmic energy factor matrix[13]-[14].

In order to calculate stress intensity factors, interaction integral method is commonly used. In general, the J-integral for a given problem can be written as

$$J = \frac{1}{8\pi}\begin{bmatrix} K_I B_{11}^{-1} K_I + 2K_I B_{12}^{-1} K_{II} + 2K_I B_{13}^{-1} K_{III} \\ +(term-not-involving-K_I) \end{bmatrix} \tag{2}$$

where *I*, *II*, *III* correspond to 1, 2, 3 when indicating the components of *B*. We define the J-integral for an auxiliary, pure mode I, crack- tip field with stress intensity factor k_I, as

$$J_{aux}^I = \frac{1}{8\pi} k_I . B_{11}^{-1} . k_I \tag{3}$$

Superposing the auxiliary field onto the actual field yields

$$J_{tot}^I = \frac{1}{8\pi}\begin{bmatrix} (K_I + k_I) B_{11}^{-1} K_I + 2(K_I + k_I) B_{12}^{-1} K_{II} \\ +2(K_I + k_I) B_{13}^{-1} K_{III} + (termnotinvolvingK_I ork_I) \end{bmatrix} \tag{4}$$

Since the terms not involving K_I or k_I in J_{tot}^I J are equal, the interaction integral can be defined as

$$J_{\text{int}}^I = J_{tot}^I - J - J_{aux}^I = \frac{k_I}{4\pi}\left[B_{11}^{-1} K_I + B_{12}^{-1} K_{II} + B_{13}^{-1} K_{III}\right] \tag{5}$$

If the calculations are repeated for mode *II* and mode *III*, a linear system of equation results:

$$J_{\text{int}}^\alpha = \frac{k_\alpha}{4\pi} B_{\alpha\beta}^{-1} K_\beta \tag{6}$$

If the k_α are assigned unit values, the solution of the above equation to

$$K = 4\pi B . J_{\text{int}} \tag{7}$$

where $J_{\text{int}} = \left[J_{\text{int}}^I, J_{\text{int}}^{II}, J_{\text{int}}^{III}\right]^T$. Based on the definition of the J-integral, the interaction integrals J_{int}^α can be expressed as

$$J_{\text{int}}^\alpha = \lim_{\Gamma\to 0} \int_\Gamma n . M^\alpha . q d\Gamma \tag{8}$$

with M^α give as

$$M^\alpha = \sigma : \varepsilon_{aux}^\alpha I - \sigma . \left(\frac{\partial u}{\partial x}\right)_{aux}^\alpha - \sigma_{aux}^\alpha \tag{9}$$

The subscript *aux* represent three auxiliary pure Mode I, Mode II, and Mode III crack-tip fields for $\alpha = I, II, II$, respectively. is a contour that lies in the normal plane at position *s* along the crack front, beginning on the bottom crack surface and ending on the top surface (Fig. 3). The limit $\Gamma \to 0$ indicates that shrinks onto the crack tip [13]-[14].

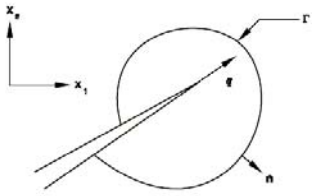

Fig. 3 Contour for calculating J-integral

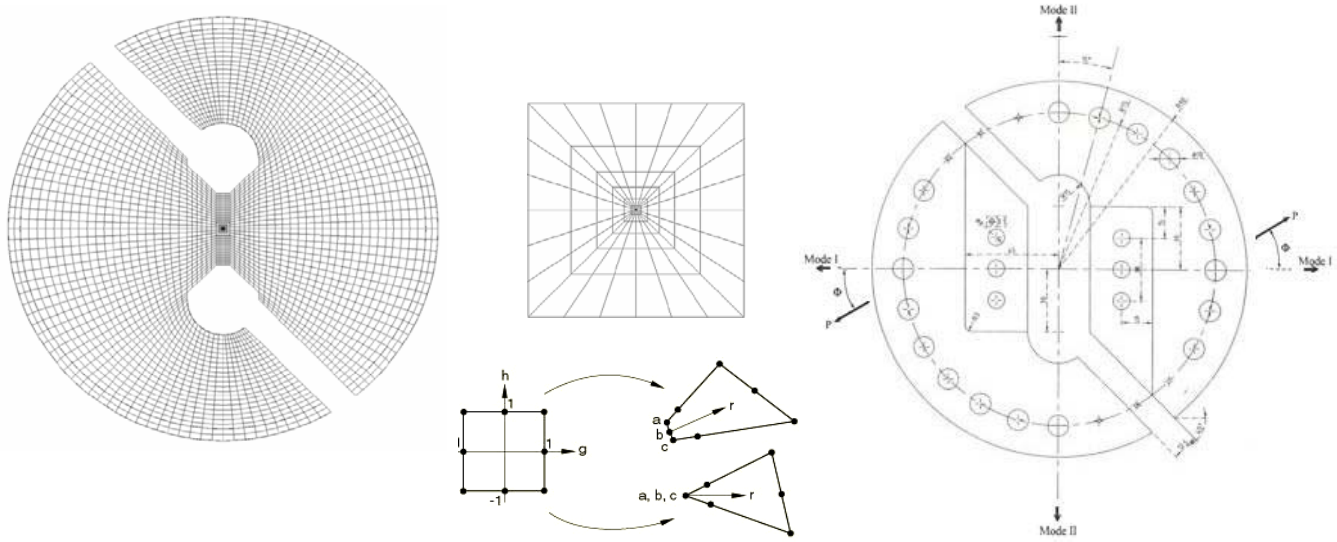

(a) (b)

Fig. 4 a) Finite element mesh pattern, b) fin mesh around the crack tip and singularity c) Arcan apparatus

III. Finite Element Modeling

Numerical analyses were carried out using the interaction *J*-integral method. Fig. 4 shows example of the mesh pattern of the specimen, which were performed with ABAQUS under a constant load of 40000 N. The entire specimen was modeled using eight node collapsed quadrilateral element and the mesh was refined around crack tip, so that the smallest element size found in the crack tip elements was approximately 0.02 mm. A linear elastic finite element analysis was performed under a plain strain condition using $1/r^{0.5}$ stress field singularity. To obtain a $1/r^{0.5}$ singularity term of the crack tip stress field, the elements around the crack tip were focused on the crack tip and the mid side nodes were moved to a quarter point of each element side.

For verification of FE modeling, the compact tension specimen of ASTM E399 standard is used. These models run in mode-I for various crack length vs. specimen width *(0.45<a/w<0.55)* and the geometric calibration factors are compared with ASTM E399 standard. The compact tension specimen and FE model are shown in Fig. 5. FE result was exactly fitted on standard curve that shown in Fig. 6.

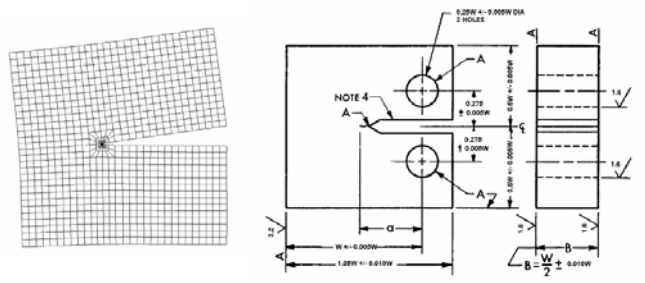

(a) (b)

Fig. 5 a) Finite element mesh pattern, b) compact tension specimen

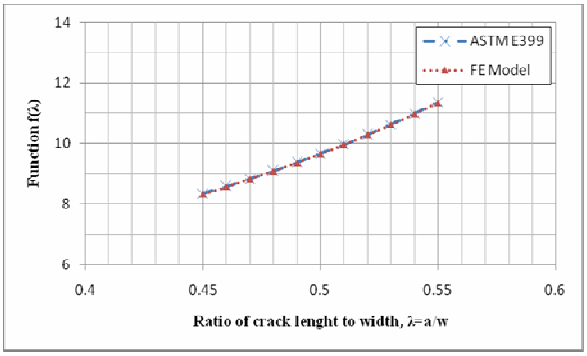

In these models, specimen width is *W=30 mm*, crack length is *0.45<a<0.55* and applied load is 40000N.

The calibration factors calculated through

$$K_I = \frac{P}{B\sqrt{w}} f(\lambda) \tag{10}$$

Where, P is the applied load, W is specimen width, B is specimen thickness and $f(\lambda)$ is geometric calibration factor.

IV. Results and Discussions

A. Mode-I & II Geometric Calibration Factors

In order to assess geometrical factors or non-dimensional stress intensity factors $f_I(a/w)$ and $f_{II}(a/w)$ to determine fracture toughness for specimens, the *a/w* ratio was varied between 0.1 and 0.8 at 0.1 intervals and a fourth order polynomial was fitted through finite element analysis for plane strain conditions as (Fig. 6):

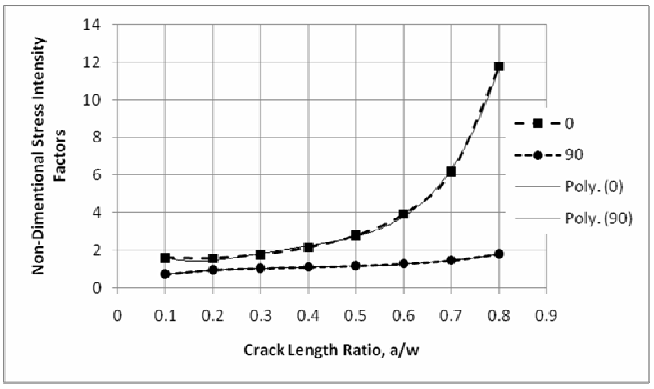

Fig. 6 Calibration Factors vs. crack length

$f_I(a/w)(\alpha=0)=188.6(a/w)^4-260.9(a/w)^3+134.2(a/w)^2+26.3(a/w)+3.16$

$f_{II}(a/w)(\alpha=90)=-2.34(a/w)^4+12.04(a/w)^3-12.07(a/w)^2+4.977(a/w)+0.348$

Here *a/w* is the crack length ratio, where *a* is the crack length and *w* is the specimen length.

The relationship between the non-dimensional stress intensity factor and the loading angle is shown in Fig. 7. It can be seen that for loading angles $\alpha \leq 67^o$, the mode-I fracture is dominant and as the mode-II loading contribution increases, the mode-I stress intensity factor decreases and the mode-II stress intensity factor increases. For $\alpha \geq 75^o$ mode-II fracture becomes dominant.

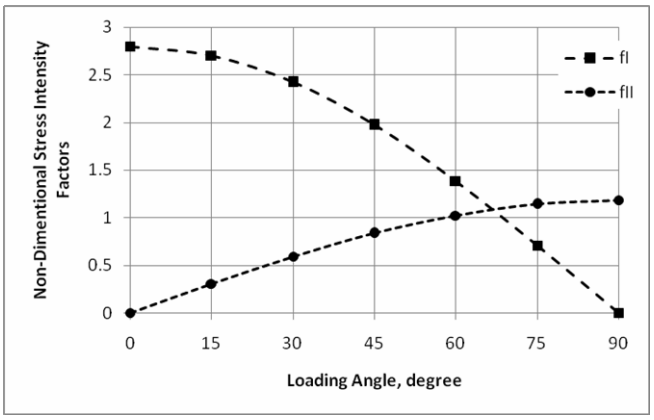

Fig. 7 Calibration Factors vs. loading angle for the crack length 15mm.

B. Mixed-Mode Geometric Calibration Factors

In order to assess geometrical factors or non-dimensional stress intensity factors for mixed-mode conditions to determine specimens fracture toughness, the *a/w* ratio was varied between 0.1 and 0.7 at 0.1 intervals in plane strain conditions are shown in Figs. 8-9 and Tables I-II. For plane strain condition the *a/w* ratio was varied between 0.45 and 0.55 at 0.01 intervals are shown in Figs. 10-11 and Tables III-IV.

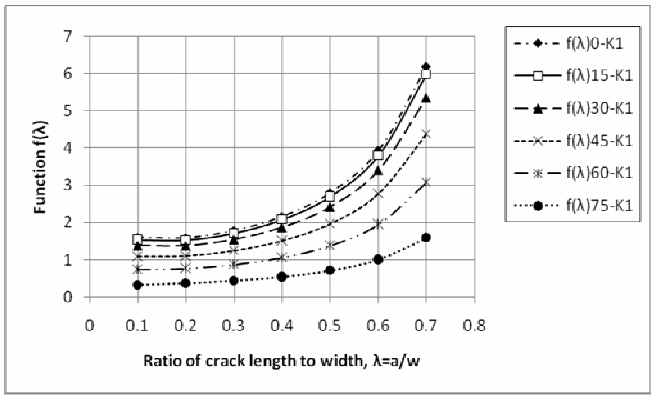

Fig. 8 Calibration Factors for *0.1<a/w<0.9* in Mode I

TABLE I
CALIBRATION FACTORS FOR *0.1<A/W<0.9* MODE I

a/w	f(λ)-K1						
	f(λ)0-K1	f(λ)15-K1	f(λ)30-K1	f(λ)45-K1	f(λ)60-K1	f(λ)75-K1	f(λ)90-K1
0.1	1.597	1.542	1.377	1.104	0.742	0.320	0
0.2	1.587	1.534	1.375	1.115	0.770	0.365	0
0.3	1.779	1.718	1.542	1.254	0.875	0.432	0
0.4	2.156	2.083	1.866	1.521	1.066	0.537	0
0.5	2.796	2.701	2.420	1.972	1.388	0.706	0
0.6	3.932	3.797	3.402	2.775	1.955	1.002	0
0.7	6.181	5.970	5.350	4.365	3.081	1.588	0
0.8	11.755	11.358	10.183	8.309	5.873	3.035	0
0.9	34.585	33.388	29.935	24.438	17.280	8.941	0

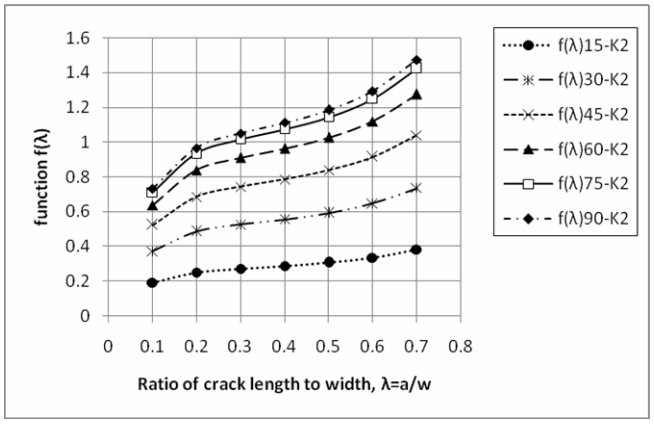

Fig. 9 Calibration Factors for 0.1<*a/w*<0.9 in Mode II

TABLE II
CALIBRATION FACTORS FOR 0.1<*A/W*<0.9 MODE I

a/w	f(λ)-K2						
	f(λ)0-K2	f(λ)15-K2	f(λ)30-K2	f(λ)45-K2	f(λ)60-K2	f(λ)75-K2	f(λ)90-K2
0.1	0	0.191	0.373	0.522	0.638	0.710	0.733
0.2	0	0.251	0.485	0.686	0.839	0.935	0.966
0.3	0	0.273	0.526	0.744	0.911	1.015	1.051
0.4	0	0.288	0.556	0.786	0.963	1.074	1.112
0.5	0	0.307	0.592	0.837	1.026	1.144	1.185
0.6	0	0.335	0.647	0.914	1.120	1.250	1.295
0.7	0	0.381	0.736	1.041	1.275	1.423	1.475
0.8	0	0.469	0.906	1.282	1.570	1.753	1.815
0.9	0	0.685	1.323	1.873	2.293	2.559	2.650

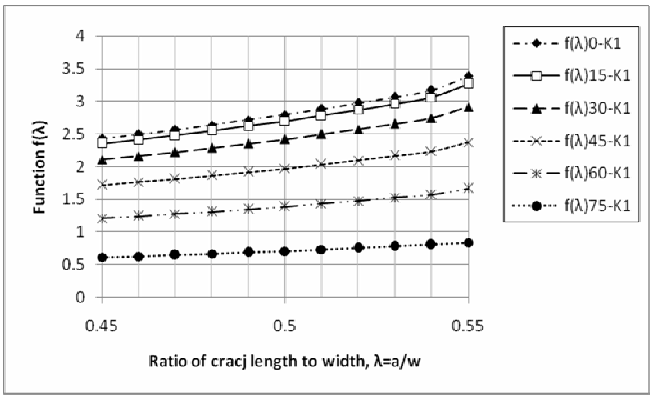

Fig. 10 Calibration Factors for 0.45<*a/w*<0.55 in Mode I

TABLE III
CALIBRATION FACTORS FOR 0.45<*A/W*<0.55 MODE I

a/w	f(λ)-K1						
	f(λ)0-K1	f(λ)15-K1	f(λ)30-K1	f(λ)45-K1	f(λ)60-K1	f(λ)75-K1	f(λ)90-K1
0.45	2.435	2.352	2.108	1.717	1.206	0.611	0
0.46	2.499	2.414	2.163	1.763	1.239	0.629	0
0.47	2.566	2.479	2.222	1.810	1.272	0.646	0
0.48	2.639	2.550	2.285	1.862	1.309	0.666	0
0.49	2.716	2.623	2.351	1.916	1.348	0.685	0
0.5	2.796	2.701	2.420	1.972	1.388	0.706	0
0.51	2.883	2.787	2.496	2.034	1.431	0.729	0
0.52	2.974	2.872	2.574	2.098	1.476	0.753	0
0.53	3.070	2.965	2.657	2.166	1.525	0.778	0
0.54	3.171	3.062	2.744	2.237	1.575	0.804	0
0.55	3.387	3.265	2.919	2.372	1.663	0.838	0

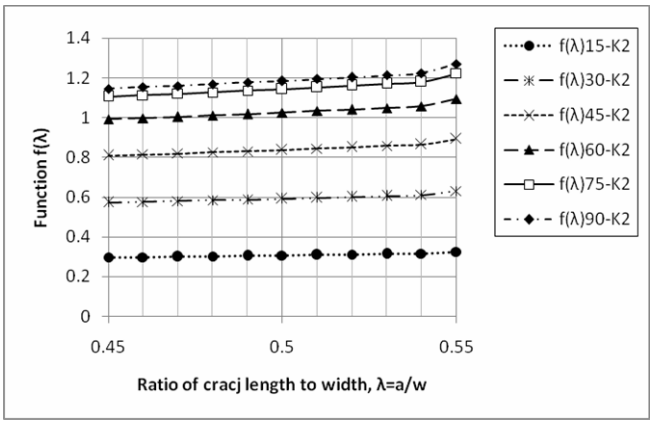

Fig. 11 Calibration Factors for 0.45<*a/w*<0.55 in Mode II

TABLE IV
CALIBRATION FACTORS FOR 0.45<*A/W*<0.55 MODE II

a/w	f(λ)-K2						
	f(λ)0-K2	f(λ)15-K2	f(λ)30-K2	f(λ)45-K2	f(λ)60-K2	f(λ)75-K2	f(λ)90-K2
0.45	0	0.297	0.573	0.810	0.992	1.106	1.146
0.46	0	0.299	0.575	0.815	0.998	1.113	1.154
0.47	0	0.301	0.580	0.820	1.004	1.121	1.161
0.48	0	0.303	0.584	0.826	1.011	1.127	1.169
0.49	0	0.305	0.588	0.832	1.019	1.137	1.178
0.5	0	0.307	0.592	0.837	1.026	1.144	1.185
0.51	0	0.309	0.597	0.844	1.034	1.153	1.195
0.52	0	0.312	0.602	0.851	1.042	1.161	1.204
0.53	0	0.314	0.607	0.857	1.050	1.172	1.214
0.54	0	0.317	0.611	0.864	1.059	1.181	1.224
0.55	0	0.324	0.630	0.892	1.095	1.223	1.270

C. Effect of Crack Length on Mixed-Mode Fracture for Steel Butt Weld for P=40000N

Strain energy versus loading angle is demonstrated in Fig. 12, an increase of loading angle from 0 to 90 leads to a reduction of strain energy and this causes an increase of fracture resistance of structure. Also a decrease of crack length ratio leads to a same effect on fracture resistance.

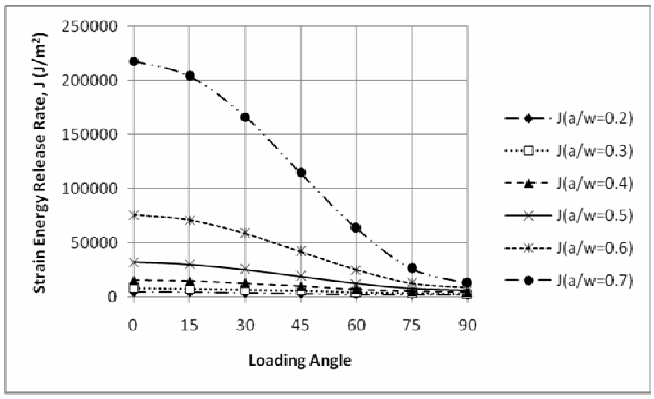

Fig. 12 Strain energy release rate vs. loading angle, P=40000N

Figs. 13 and 14 show the effect of increasing of loading angle and crack length ratio on stress intensity factors of mode-I and mode-II.

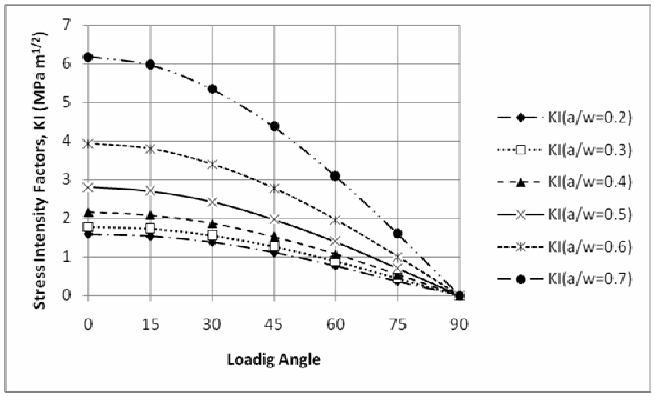

Fig 13 Mode-I stress intensity factor vs. loading angle for different crack length ratio, P=40000N

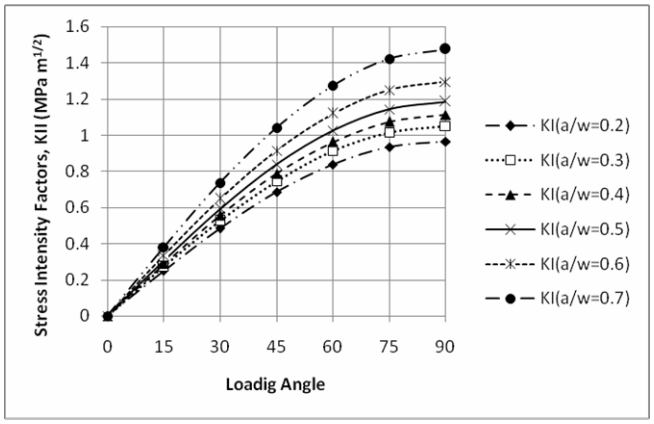

Fig 14 Mode-II stress intensity factor vs. loading angle for different crack length ratio, P=40000N

D. Effect of Mixed-Mode Ratio

In Fig. 15 the strain energy release rate for pure mode-I and pure mode-II and also total release energy are demonstrated. The total strain energy release rate under mixed-mode loading condition decreases with the loading angle. Therefore, the increase of the mode-II loading contribution leads to a reduction in the total strain energy release rate.

The relationship between strain energy release rate and mixed-mode ratio is showed in Fig. 16.

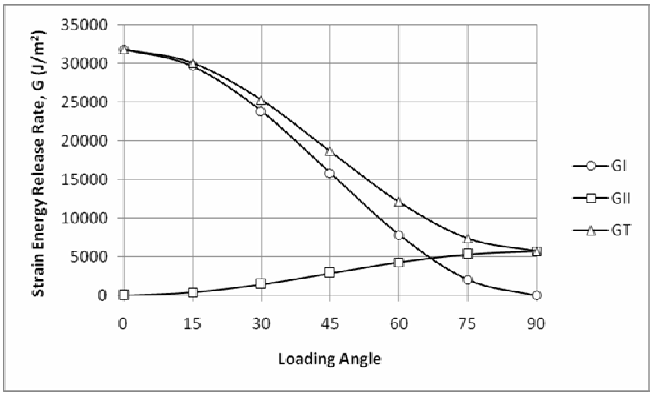

Fig 15 Strain energy release rate of mode-I (G_I), mode-II (G_{II}) and total strain energy (G_T) vs. loading angle

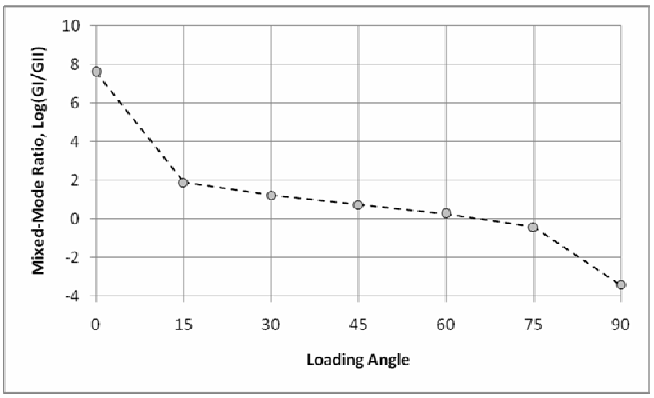

Fig. 16 The ratio of mode-I to mode-II, G_I/G_{II}, in logarithmic scale vs. loading angle

V. Conclusion

In this paper, the mixed mode fracture mechanics parameters were investigated for high tensile steel butt welded joint for modified Arcan test specimen and finite element analysis was used to evaluate the effect of crack length on fracture criterion. The geometric calibration factors were given for both plane stress and plane strain conditions and different mixed-mode loading conditions of modified Arcan specimen. The results of this study will be used in future investigations on mixed mode fracture of high tensile steel butt welded joint through experimental analysis.

References

[1] Lawn BR, Wilshaw TR. Fracture of brittle solids. London: Cambridge University Press, 1975.

[2] Michael A. Sutton, Michael L. Boone, Fashang Ma, Jeffrey D. Helm, A combined modeling-experimental study of the crack opening displacement fracture criterion for characterization of stable crack growth under mixed mode I/II loading in thin sheet materials; Engineering Fracture Mechanics 66 (2000) 171-185

[3] Wilkins, D. J.; Eisenmann, J. R.; Camin, R. A.; Margolis, W. S.; Benson, R. A.; Characterizing Delamination Growth in Graphite-Epoxy, Damage in Composite Materials, ASTM STP 775, K. L. Reifsnider, Ed., American Society for Testing and Materials, Philadelphia, 1982, pp. 168-183.

[4] American Society for Testing and Materials. 2007. Standard E399-06, Standard Test Method for Linear-Elastic Plane-Strain Fracture Toughness KIC of Metallic Materials. Annual Book of ASTM Standards. Philadelphia: ASTM.

[5] Russell, A. J.; On the Measurement of Mode II Interlaminar Fracture Energies, DREP Materials Report. 82-0, Defense Research Establishment Pacific, Victoria, December, 1982.

[6] O'Brien, T. K.; Mixed-Mode Strain-Energy-Release Rate Effects on Edge Delamination of Composites, Effects of Defects in Composite Materials, ASTM STP 836, D. J. Wilkins, Ed., American Society for Testing and Materials, Philadelphia, 1984, pp. 125-142.

[7] Johnson, W. S.; Stress Analysis of the Crack-lap-Shear Specimen: An ASTM Round-Robin, Journal of Testing and Evaluation, JTEVA, Vol. 15, No.6, November 1987, pp. 303-324.

[8] Reeder, J. R.; and Crews, J. H., Jr.; The Mixed-Mode Bending Method for Delamination Testing, AIAA Journal, Vol. 28, No.7, July 1990, pp. 1270-1276.

[9] Bradley, W. L.; and Cohen, R. N.; Matrix Deformation and Fracture in Graphite-Reinforced Epoxies, Delamination and Debonding of Materials, ASTM STP 876, W. S. Johnson, Ed., American Society for Testing and Materials, Philadelphia, 1985, pp. 389-410.

[10] Russell, A J.; and Street, K. N.; Moisture and Temperature Effects on the Mixed-Mode Delamination Fracture of Unidirectional Graphite/Epoxy, Delamination and Debonding of Materials, ASTM STP 876, W. S. Johnson, Ed., American Society for Testing and Materials, Philadelphia, 1985, pp. 349-370.

[11] Hashemi, S.; Kinloch, A. J.; and Williams J. G.; Interlaminar Fracture of Composite Materials, 6th ICCM & 2nd ECCM Conference Proceedings, Vol. 3, London, July 1987, pp. 3.254-3.264.

[12] Arcan, M.; Hashin, Z.; and Voloshin, A., A Method to Produce Uniform Plane- Stress States with Applications to Fiber-Reinforced Materials, Experimental Mechanics, Vol. 28, April 1978, pp. 141-146.

[13] Naghdali Choupani. "Experimental and numerical investigation of the mixed mode delamination in Arcan laminated specimens." Material science and technology, volume 478: 229-242,2008.

[14] ABAQUS user's manual, version 6.5. Pawtucket, USA: Hibbit, Karlsson and Sorensen, HKS Inc; 2004.